Intervalenceband and plasmon optical absorption in heavily doped GaAs:C

W. Songprakob, R. Zallen, D. V. Tsu, and W. K. Liu

Articles you may be interested in

Optical characterizations of heavily doped p -type Al x Ga 1 − x As and GaAs epitaxial films at terahertz frequencies
J. Appl. Phys. **97**, 093529 (2005); 10.1063/1.1894581

Carbon reactivation kinetics in GaAs: Its dependence on dopant precursor, doping level, and layer thickness
J. Appl. Phys. **91**, 5923 (2002); 10.1063/1.1467953

Effect of growth rate on surface morphology of heavily carbon-doped InGaAs
J. Vac. Sci. Technol. B **19**, 1550 (2001); 10.1116/1.1374622

Characterization of heavily carbon-doped InGaAsP layers grown by chemical beam epitaxy using tetrabromide
Appl. Phys. Lett. **73**, 2482 (1998); 10.1063/1.122489

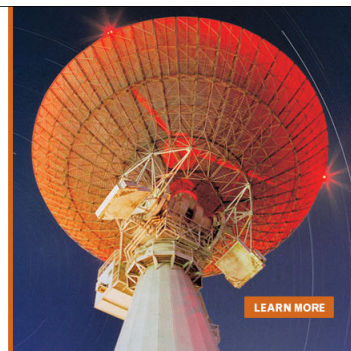Infrared study of light-induced reactivation of neutralized dopants in hydrogenated n-type GaAs doped with silicon
Appl. Phys. Lett. **73**, 644 (1998); 10.1063/1.121934

Intervalenceband and plasmon optical absorption in heavily doped GaAs:C

W. Songprakob and R. Zallen[a)]
Department of Physics, Virginia Tech., Blacksburg, Virginia 24061-0435

D. V. Tsu
Energy Conversion Devices, Incorporated, Troy, Michigan 48084

W. K. Liu
IQE Incorporated, Bethlehem, Pennsylvania 18015

By using direct numerical-solution techniques for the reflectance (R) and transmittance (T) equations of a multilayer structure, we have analyzed infrared R and T measurements on heavily doped p-type GaAs:C films grown by molecular beam epitaxy. The optical properties, for films with hole concentrations up to 1.4×10^{20} cm^{-3}, were determined for photon energies from 0.07 to 0.6 eV, in which region plasmon (intraband) and intervalenceband contributions are in competition. Our results for the optical absorption coefficient resolve two separate peaks located (at high doping) at about 0.1 and 0.2 eV. By carrying out calculations of the intervalenceband (IVB) absorption processes for our dopings, we identify the peak near 0.2 eV with light-hole to heavy-hole IVB transitions, and we attribute the lower-energy peak to hole-plasmon excitations. Our experimental absorption spectra are very well described by a model combining the IVB contribution to the dielectric function with a plasmon contribution. The hole-plasmon parameters we obtain for highly doped p-GaAs yield an infrared mobility which (unlike the too-small IVB-entangled infrared mobility implied by the use of the usual effective-plasmon model) is in substantial agreement with the dc mobility. © *2002 American Institute of Physics.* [DOI: 10.1063/1.1424050]

I. INTRODUCTION

In 1962 Braunstein and Kane,[1] in a classic experimental and theoretical study of lightly doped p-type GaAs, observed three infrared absorption bands and identified them with intervalenceband (IVB) transitions among the heavy-hole (hh), light-hole (lh), and spin–orbit split-off (so) bands. For heavily doped p-GaAs, infrared studies have focused on hole-plasmon processes (free-carrier intraband transitions) as manifested in the doping dependence of a highly damped reflectivity plasma edge.[2,3] (The plasmonlike L_+ mode is, in p-GaAs, inaccessible to Raman experiments.[3]) Absorptance measurements on heavily doped p-GaAs films grown by molecular beam epitaxy (MBE) were reported recently by Songprakob *et al.*[3] and by Huberman *et al.*[4] Both groups recognized that intervalenceband transitions contribute significantly to infrared absorption, but their results suggest only one very broad absorption feature which is a combination of hole-plasmon and IVB contributions. The thin-film/substrate sample geometry complicates extraction of the optical properties directly from the experimental measurements. In Ref. 3 (henceforth, SZLB), a simple two-parameter effective-plasmon model was found to adequately describe the reflectance (R) and transmittance (T) data, and the optical properties were then derived from the model. But since the conventional effective-plasmon model here represents a broad absorption continuum including both true-plasmon and IVB contributions, the effective-plasmon damping parameter is quite large so the optical hole mobility

(which is operationally defined by this model) is small. This is the reason for the observed dichotomy between the infrared mobility and the dc (Hall) mobility in p-GaAs.

In the present work, we report model-independent experimental determination of the optical properties of heavily doped MBE-grown GaAs:C thin films, using a recently developed numerical-solution technique for handling the nonlinear R and T equations of an (air/film/substrate/air) structure.[5] This approach, embodied in software (*OptiCon*) developed by Tsu,[6] combines a graphical technique with Newton–Raphson iteration.[7] At each wavelength, this technique uses the measured (R,T) values to determine (n,k), the refractive index and extinction coefficient. (n,k) then determine the other optical properties, including the optical absorption coefficient α. In addition to providing a direct path from the experimental data to the optical properties of the film (without an intervening model dielectric function), the technique is also found to be useful for providing, as a valuable by-product, an accurate independent estimate of the film's thickness.[5,8] The resulting experimental spectra reveal, for the optical properties of heavily doped p-GaAs films, two separate peaks in $\alpha(h\nu)$. By carrying out band-structure calculations of the intervalenceband absorption processes, we identify the higher-energy peak (near 0.2 eV at our highest doping) with light-hole to heavy-hole IVB transitions, and we attribute the lower-energy peak to the hole plasmon. The hole-plasmon parameters we obtain for highly doped p-GaAs yield an infrared mobility which (unlike the IVB-entangled effective-plasmon infrared mobility) is in substantial agreement with the dc mobility.

[a)]Electronic mail: rzallen@vt.edu

     171

TABLE I. The second and third columns give the hole concentration (Hall effect) and intended (growth-rate) thickness of each MBE GaAs:C film. The *OptiCon* thickness was determined from our reflectance and transmittance measurements using the numerical technique we have described. The last two columns give the peak height and peak position of the experimentally determined absorption band (Figs. 2 and 3) that is identified with light-hole to heavy-hole intervalenceband transitions.

Sample	p (10^{18} cm^{-3})	Thickness (nm)		$\alpha_{lh \to hh}$ (10^4 cm^{-1})	$h\nu_{lh \to hh}$ (eV)
		MBE	OptiCon		
(e)	20	750	739	0.9	0.14
(f)	27	500	519	1.2	0.15
(g)	33	500	517	1.4	0.15
(h)	66	500	505	2.5	0.16
(i)	82	500	513	3.0	0.17
(j)	91	350	346	3.2	0.18
(k)	110	500	507	3.6	0.19
(l)	140	500	520	4.0	0.20

Experimental aspects are given in Sec. II. The numerical/graphical analysis of our infrared R and T data is described in Sec. III, which presents results for the optical properties of the GaAs:C films. The inadequacy of the effective-plasmon approach for p-GaAs is briefly discussed in Sec. IV. Our procedure for disentangling the intervalenceband and the true-plasmon contributions is described in Sec. V. Section V also contains our calculations, at various dopings, of the spectral form of the intervalenceband contribution to the dielectric function. When combined with the plasmon contribution, excellent fits to the experimental (R,T)-determined optical spectra are obtained. The implications for the genuine hole-plasmon properties of highly doped p-GaAs are stated in Sec. VI. In Sec. VII we summarize our main findings.

II. EXPERIMENT

Measurements were made on eight MBE-grown GaAs:C films with hole concentrations ranging from 2.0×10^{19} to 1.4×10^{20} cm^{-3}. The film thickness was 500 nm for six films, 350 nm for one film, and 750 nm for one film; the semi-insulating GaAs substrate thickness was 635 μm. The growth procedure is described in Ref. 3, which also gives a detailed discussion of the Hall-derived hole concentrations p_{Hall} and hole mobilities μ_{Hall} for the films. Reflectance and transmittance measurements on the film-on-substrate samples were carried out at room temperature using a Bomem DA3 Fourier-transform spectrometer.[3] R and T was determined at each of 2300 points (photon energies) between 550 cm^{-1} (0.07 eV) and 5000 cm^{-1} (0.62 eV). This frequency regime, which is above the one-phonon and two-phonon regions and well below the band gap, is very transparent in intrinsic GaAs. But in p-type GaAs, this frequency regime is filled with hole-plasmon and intervalenceband processes. The measured reflectance (R) and absorptance $(1-R-T)$ spectra are shown in Ref. 3.

The film thicknesses given above were growth-rate determined using MBE growth rates established by both high-resolution x-ray diffraction and reflection high-energy electron diffraction measurements carried out on calibration AlGaAs/GaAs superlattice structures. As described below, the work reported here provides additional independent de-

termination of film thickness. The two determinations, listed in Table I, agree well. Table I also lists the carrier concentrations of the films.

III. DETERMINATION OF THE OPTICAL PROPERTIES OF THE GaAs:C FILMS

The (air/film/substrate/air) structure yields R and T equations[3,5] which are very nonlinear in n and k as well as in the film thickness d. At each photon-energy point, we used these equations to numerically determine (n,k) from the measured reflectivity and transmittance. (n,k) can be solved for by Newton–Raphson iteration.[5–9] This technique requires an initial (n_i, k_i) value and the expansions of the R and T equations up to first order in $(\Delta n, \Delta k)$:

$$R(n_i, k_i, d) + \frac{\partial R}{\partial n}\Delta n + \frac{\partial R}{\partial k}\Delta k = R_{measured}, \quad (1)$$

$$T(n_i, k_i, d) + \frac{\partial T}{\partial n}\Delta n + \frac{\partial T}{\partial k}\Delta k = T_{measured}. \quad (2)$$

With a reasonable initial value, $(n_i + \Delta n, k_i + \Delta k)$ usually converges to a solution after a few iterations. Complementing the iteration technique, (R,T)-determined plots in the (n,k) domain help to identify the numerical solutions. One plot is the locus of all (n,k) pairs for which $R(n,k) = R_{measured}$; the other is the locus of all (n,k) pairs for which $T(n,k) = T_{measured}$. These two curves generally intersect at two points; one (n,k) solution is nonphysical, "extra," an artifact of the mathematical form of $R(n,k)$ and $T(n,k)$.

The thickness d_s (635 μm for our samples) and the optical constants (n_s, k_s) of the GaAs substrate are required in the R and T equations as well. The substrate optical constants were obtained from the bulk GaAs lattice dielectric function: $\epsilon_{lattice} = \epsilon_\infty + \epsilon_\infty (\omega_{LO}^2 - \omega_{TO}^2)/(\omega_{TO}^2 - \omega^2 + i\omega\Gamma)$, where $\epsilon_\infty = 10.9$, $\omega_{TO} = 268$ cm^{-1}, $\omega_{LO} = 292$ cm^{-1}, and $\Gamma = 2.5$ cm^{-1}. (ϵ_∞, ω_{TO}, and ω_{LO} are from Ref. 10; Γ is from Ref. 11.) n_s is nearly constant (close to 3.3) throughout our infrared region of interest, and k_s is essentially zero. (This is a highly transparent region for intrinsic GaAs, since it contains no first-order or second-order phonon processes as well as no interband transitions.)
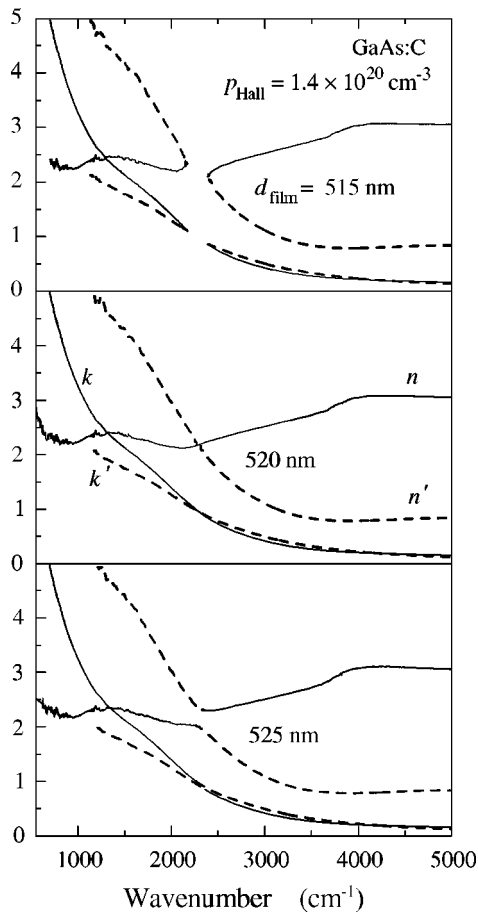
FIG. 1. (R,T)-determined optical constants for the most highly doped GaAs:C film for three trial values of the film thickness. The curves (n,k) and (n',k') correspond to the physical and extra numerical solutions, respectively. The middle panel represents our results for d_{film}, $n(h\nu)$, and $k(h\nu)$.

Figure 1 shows optical-constant solutions corresponding to the experimental R and T for the highest doping ($p_{Hall} = 1.4 \times 10^{20}$ cm^{-3}), using iteration of Eqs. (1) and (2) with three trial values of the film thickness d. The physical (n,k) solutions (the spectra represented by the solid lines) are easily distinguished from the extra (n',k') solutions (dotted lines) by a comparison to n_s. The film thickness d is a free parameter, and the curves (n,k) and (n',k') are sensitive to its value. Their crossing topology is dependent on d. When d is underestimated (515 nm), there is no solution in the frequency region of 2100–2400 cm^{-1}, and the no-solution frequency gap gets bigger for smaller d. When d is overestimated (525 nm), the physical and the extra spectral curves are again discontinuous, now displaced vertically. The change in topology, from a horizontal gap to a vertical one, occurs at the correct d (520 nm). Here the gap disappears, and the physical n curve is continuous and crosses the extra n' curve (similarly for the k and k' curves.) For each sample, the film thickness at the crossing transition [referred to here as the *OptiCon* thickness or the (R,T)-determined thickness] was determined and the physical (n,k) was then accurately extracted from the measured R and T at each photon energy. The (R,T)-determined thicknesses of the eight samples are given in Table I, along with the MBE-growth-rate thick-
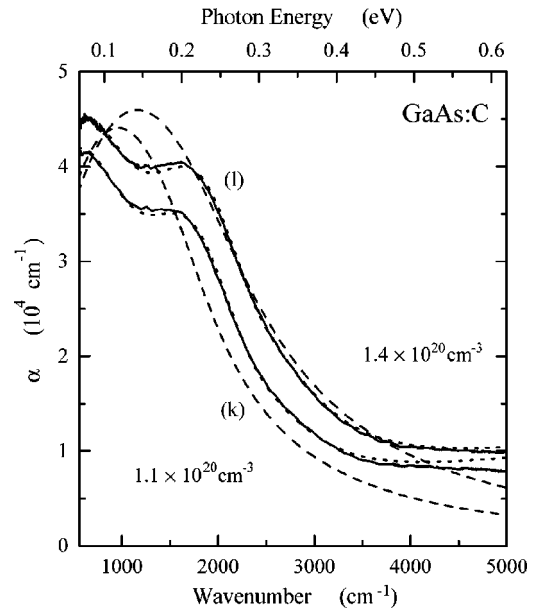

FIG. 2. Experimental absorption coefficient $\alpha(h\nu)$ (solid lines), for samples (k) and (l), extracted from the experimental R and T using the direct numerical-solution technique. Shown as dashed lines are the $\alpha(h\nu)$ curves corresponding to the effective-plasmon model. The dotted lines (nearly indistinguishable here from the solid lines) correspond to a dielectric function which explicitly includes an intervalenceband contribution as well as a plasmon contribution.

nesses. The two thicknesses agree to within 4% in each case. Thus, in addition to yielding the optical constants (n,k) of the film, this direct numerical-solution technique can be used to closely determine the film thickness.

Using $\alpha = 4\pi\nu k/c$, the absorption coefficient $\alpha(h\nu)$ at each photon energy $h\nu$ was then determined from the numerical solution for $k(h\nu)$. The $\alpha(h\nu)$ results, for four of the highly doped GaAs:C films, are given by the solid lines in Figs. 2 and 3. At high doping ($p_{Hall} > 6 \times 10^{19}$ cm^{-3}), $\alpha(h\nu)$ reveals two separate, broad peaks at about 0.1 and 0.2 eV. We identify the lower-energy peak as the actual plasmon peak $\alpha_{plasmon}$, and the higher-energy one as the intervalenceband light-hole-to-heavy hole (IVB lh→hh) peak $\alpha_{lh→hh}$.

In comparison to the $\alpha(h\nu)$ observed by Braunstein and Kane[1] on lightly doped p-type GaAs:Zn ($p_{Hall} = 3 \times 10^{17}$ cm^{-3}), the lh→hh IVB absorption band is much stronger in our heavily doped samples, while the partially resolved so→lh and so→hh absorption bands, seen in their lightly doped p-type GaAs at about 0.3 and 0.4 eV, respectively, are stronger but are broadened nearly beyond recognition in heavily doped p-type GaAs. Similar severe broadening of IVB absorption bands has been observed for heavily doped p-type Ge.[12]

IV. LIMITATIONS OF THE EFFECTIVE-PLASMON MODEL FOR *p*-GaAs

In the standard infrared analysis for free carriers (electron or holes), a reflectivity plasma edge is fit using a Drude-model free-carrier dielectric-function contribution characterized by plasma frequency ω_p and plasma damping constant γ_p. The optical constants are then derived from the dielectric
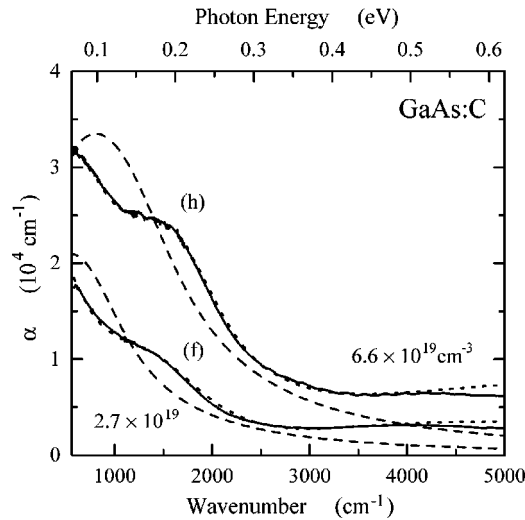
FIG. 3. Experimental absorption coefficient $\alpha(h\nu)$ (solid lines), for samples (f) and (h), extracted from the experimental R and T using the direct numerical-solution technique. Shown as dashed lines are the $\alpha(h\nu)$ curves corresponding to the effective-plasmon model. The dotted lines (nearly indistinguishable here from the solid lines) correspond to a dielectric function which explicitly includes an intervalenceband contribution as well as a plasmon contribution.

function $\epsilon_{lattice} - \epsilon_\infty \omega_p^2/(\omega^2 - i\omega\gamma_p)$. This procedure was carried out for the observed reflectivity spectra of our GaAs:C samples, as reported in Ref. 3 (SZLB). The very broad reflectivity minimum seen at high dopings required a large damping constant γ_p in this effective-plasmon description. No explicit consideration of the intervalenceband contribution was included. Instead, the IVB contribution was implicitly folded into the two effective-plasmon parameters, ω_p and γ_p. The $\alpha(h\nu)$ curves corresponding to the effective-plasmon fits are shown as dashed curves in Fig. 2. The effective-plasmon $\alpha(h\nu)$ necessarily contains just a single broad band. It is seen to approximately span the region covered by the two bands resolved by our numerical analysis of the experimental (R,T) data. For such a simple two-parameter phenomenological model, it actually does a reasonable job of representing the overall behavior of the experimental $\alpha(h\nu)$. But it is of course unable to capture the two-peak character of the actual $\alpha(h\nu)$. That two-peak character arises from the parallel plasmon and intervalenceband absorption processes.

Although the effective-plasmon model is standard operating procedure for analyzing infrared reflectivity spectra of doped semiconductors, we see that it cannot be straightforwardly applied to *p*-GaAs (or, in fact, to other III–Vs with similar valenceband structure) because the quantities ω_p and γ_p so obtained do not accurately reflect the properties of the real hole plasmon. These effective-plasmon parameters are significantly influenced by the intervalenceband contribution to the optical absorption. The damping constant γ_p is especially affected; it is large because the single effective-plasmon absorption band must be broad [in its attempt to mimic the observed $\alpha(h\nu)$] in order to span the region covered by the real-plasmon and the IVB absorption bands. This large γ_p translates into a small "infrared mobility" μ_{IR}, via

$\mu_{IR} = (e/m_h^*)(1/\gamma_p)$. (Note that the infrared mobility is operationally obtained within the context of the effective-plasmon model.) This is the reason for the discrepancy between the infrared and Hall mobilities in *p*-GaAs; μ_{IR} obtained in this way is about half as large as μ_{Hall}.[2,3] In *n*-GaAs, in which interband absorption is absent in the infrared region of the plasmon reflectivity feature, the standard IR-reflectivity effective-plasmon analysis yields a μ_{IR} which does not disagree with μ_{Hall}.

V. DISENTANGLEMENT OF THE INTERVALENCEBAND AND THE PLASMON CONTRIBUTIONS

For *p*-GaAs, the effective-plasmon quantities (ω_p, γ_p, μ_{IR}) of the previous paragraph arise from an admixture of plasmon and interband processes. In order to extract properties that are representative of the true hole-gas plasmon from the experimental absorption spectra of Figs. 2 and 3, we have carried out a fitting procedure which incorporates calculation of the intervalenceband contribution to the optical dielectric function. The IVB calculation is based on Kane's $\mathbf{k} \cdot \mathbf{p}$ and $\mathbf{A} \cdot \mathbf{p}$ theories,[13] $\mathbf{k} \cdot \mathbf{p}$ theory for the valenceband structure, $\mathbf{A} \cdot \mathbf{p}$ theory for the intervalenceband optical matrix elements. The inputs to the calculation include four band-structure quantities for GaAs, the $\mathbf{k}=0$ spin–orbit splitting Δ_{so} to the split-off valence band (0.34 eV, from Ref. 10) and the three $\mathbf{k} \cdot \mathbf{p}$ valenceband parameters (L, M, and N). Fermi–Dirac statistics are also included for holes at room temperature. In addition, there is one adjustable parameter in the IVB portion of the optical dielectric function, a broadening (damping) constant γ_{IVB} for the IVB processes. To complete the dielectric function, we add the Drude-model term with plasmon parameters $\omega_{plasmon}$ and $\gamma_{plasmon}$, where $\omega_{plasmon}$ and $\gamma_{plasmon}$ more realistically represent the properties of the actual hole plasmon than do ω_p and γ_p. (The true-plasmon quantities are denoted by $\omega_{plasmon}$ and $\gamma_{plasmon}$ to distinguish them from the effective-plasmon ones ω_p and γ_p.) The total dielectric function thus contains three adjustable parameters (γ_{IVB}, $\omega_{plasmon}$, and $\gamma_{plasmon}$). These quantities are determined by minimizing $\Sigma|\alpha_{measured} - \alpha_{calculated}|^2$, where $\alpha_{measured}$ is the experimentally observed absorption coefficient of Figs. 2 and 3 and $\alpha_{calculated}$ is obtained from the dielectric function $\epsilon_{lattice} + \epsilon_{IVB} + \epsilon_{plasmon}$ containing the IVB calculation and the plasmon contribution and the parameters γ_{IVB}, $\omega_{plasmon}$, and $\gamma_{plasmon}$.

For the (L, M, N) valenceband parameters of GaAs, we make use of a recent compilation of reported values that were given in Ref. 14. Among those sets of values, the three listed in Table II (those reported by Balslev,[15] by Skolnick *et al.*,[16] and by Ekardt *et al.*[17]), when used in the IVB calculation, yield excellent fits to the measured $\alpha(h\nu)$. The best fit is achieved with the results of Ekardt *et al.*[17] given, in terms of $\hbar^2/2m$, in the first column of the last row of Table II. Fixing the band-structure parameters at these values, the $E(\mathbf{k})$ curves for the heavy-hole, light-hole, and split-off bands are determined. The intervalenceband contribution $\epsilon_{IVB}(h\nu)$ to the dielectric function was then calculated using Kane's method,[13,18] yielding a function containing the damping parameter γ_{IVB}. The total dielectric function was then

TABLE II. The values of $\omega_{plasmon}$, $\gamma_{plasmon}$, and γ_{IVB} for the GaAs:C film with $p = 1.4 \times 10^{20}$ cm^{-3}, for three published sets of the GaAs (L, M, N) band-structure parameters. SD is the value of the minimized standard deviation of ($\alpha_{measured} - \alpha_{calculated}$) and $\bar{\alpha}$ is 2.4×10^4 cm^{-1}, the average absorption coefficient between 0.07 and 0.62 eV.

L, M, N ($\hbar^2/2m$)	$\omega_{plasmon}$ (cm^{-1})	$\gamma_{plasmon}$ (cm^{-1})	γ_{IVB} (cm^{-1})	SD/$\bar{\alpha}$
$-16.89, -3.21, -17.28$[a]	1580	570	1030	0.016
$-16.98, -3.48, -17.28$[b]	1570	490	930	0.028
$-17.45, -3.35, -18.00$[c]	1570	520	1000	0.014

[a]From Ref. 15.
[b]From Ref. 16.
[c]From Ref. 17.

used to determine $\alpha_{calculated}(h\nu)$, and the fit to the experimental $\alpha_{measured}(h\nu)$ was used to determine γ_{IVB}, $\omega_{plasmon}$, and $\gamma_{plasmon}$.

For the four samples in Figs. 2 and 3, the calculated $\alpha(h\nu)$ curves are the hard-to-see dotted lines which are nearly indistinguishable from the measured ones. A clearer comparison, for the most highly doped sample, is shown at the top of Fig. 4, where the continuous curve labeled Ekardt *et al.* is $\alpha_{calculated}(h\nu)$ and the points denote the (R, T)-determined $\alpha_{measured}(h\nu)$. Also included in Fig. 4 is a similar comparison carried out using the band parameters of Skolnick *et al.* for $\alpha_{calculated}(h\nu)$, illustrating the small but noticeable preference, in this optical study, for the Ekardt *et al.* values. None of the other sets of band parameters compiled in Ref. 14 fits our infrared results as well as the three sets listed in Table II. We adopted the Ekardt *et al.* values for use in analyzing the results of all our samples.
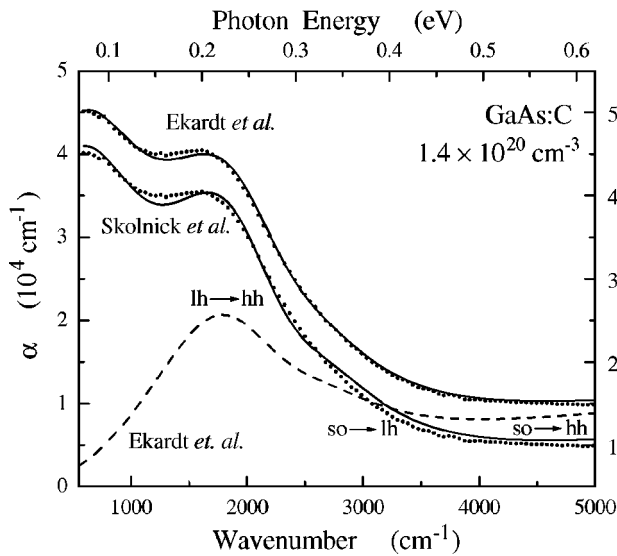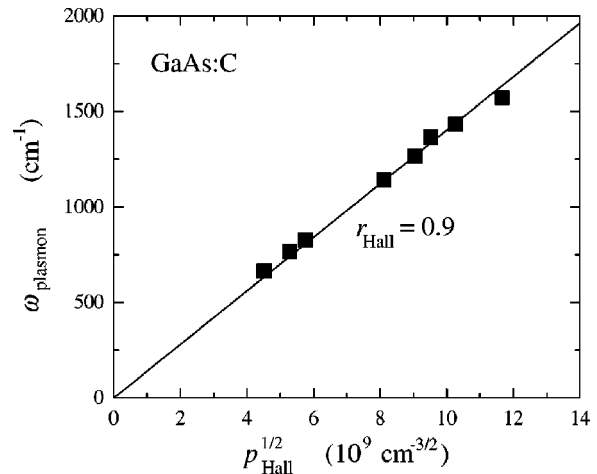

FIG. 5. Dependence of plasma frequency on the square root of the Hall-derived hole concentration. The slope corresponds to a Hall factor of 0.9.

Figure 4 shows that the two broad peaks seen at high doping in the experimental absorption spectrum are reproduced well by the calculation specified by the quantities in the last row of Table II. The broad peak centered near 0.2 eV is seen to arise from interband transitions from the light-hole to the heavy-hole valence band. This is demonstrated by the dashed curve in Fig. 4, which shows the $\alpha(h\nu)$ corresponding to ϵ_{IVB} alone. Similarly, using the $\alpha(h\nu)$ corresponding to $\epsilon_{plasmon}(h\nu)$ alone, the broad peak near 0.1 eV is seen to arise from the plasmon contribution to the dielectric function. The last column of Table I shows that the IVB peak shifts upward with an increase in doping. As the Fermi energy moves deeper into the valence band, the lh→hh transitions occur at larger $\mathbf{k}$, where $E_{hh}(\mathbf{k})$-$E_{lh}(\mathbf{k})$ increases to about 0.2 eV.

VI. HOLE-PLASMON PROPERTIES OF HIGHLY DOPED GaAs:C

Having separated, in the manner described, the plasmon and intervalenceband contributions to the observed absorption spectrum, we now examine the quantities $\omega_{plasmon}$ and $\gamma_{plasmon}$. These should more accurately describe the actual hole plasmon in GaAs:C than the IVB-entangled effective-plasmon quantities reported earlier for these samples.[3] Our results for $\omega_{plasmon}$ and $\gamma_{plasmon}$ are shown in Figs. 5 and 6.

Figure 5 presents a plot of $\omega_{plasmon}$ vs $p_{Hall}^{1/2}$, where the subscript "Hall" was added to denote the experimentally measured (Hall effect) hole concentration in Table I. Figure 6 presents a plot of μ_{IR}/μ_{Hall}, where μ_{Hall} is the measured Hall mobility and μ_{IR} is obtained from

FIG. 4. Comparison, for sample (l), of the experimental absorption spectrum (closed dots) with calculated spectra (continuous lines) which use, for the intervalenceband dielectric-function contribution, the band parameters of Skolnick *et al.* (Ref. 16) and of Ekardt *et al.* (Ref. 17). (The comparison to the work of Skolnick *et al.* corresponds to the vertically shifted scale on the right.) The dashed line represents the IVB contribution alone, obtained by omitting the plasmon contribution to the dielectric function. Heavy-hole, light-hole, and split-off valence bands are denoted hh, lh, and so, respectively, and indicate regions in which specific IVB transitions are dominant.

$$\mu_{IR} = \frac{e}{m_h^* \gamma_{plasmon}}. \tag{3}$$

Here m_h^* is $0.38m$, obtained by using the directionally averaged density-of-state masses $m_{hh} = 0.50m$ and $m_{lh} = 0.088m$ for the heavy and the light holes[10] and the expression for the two-band transport mass $m_h^* = (m_{hh}^{3/2} + m_{lh}^{3/2})/(m_{hh}^{1/2} + m_{lh}^{1/2})$.[19]
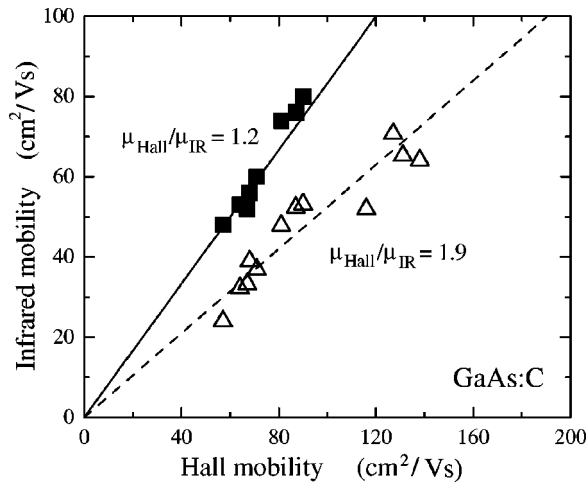
FIG. 6. Hall mobility μ_{Hall} plotted vs the optically derived infrared mobility μ_{IR}. The closed squares correspond to the present work, in which the hole-plasmon properties were determined by removing the intervalenceband contribution from the (R,T)-determined optical dielectric function. The open triangles correspond to the effective-plasmon parameters obtained for this series of samples in Ref. 3. For p-GaAs, the effective-plasmon model over-estimates the plasmon damping and thus underestimates the infrared mobility.

The results in Fig. 5 exhibit the linear relationship between the square of the plasma frequency and the carrier concentration expected,

$$\omega_{plasmon}^2 = \frac{4\pi p e^2}{\epsilon_\infty m_h^*}. \qquad (4)$$

In Eq. (4), p is the actual hole concentration, which is given by $r_{Hall} p_{Hall}$ where r_{Hall} is the Hall factor.[2,3,20,21] The Hall factor also intervenes in the connection between the actual drift mobility μ and the measured Hall mobility μ_{Hall}, $\mu = (1/r_{Hall})\mu_{Hall}$.

From Eq. (4) and $p = r_{Hall} p_{Hall}$ and the measured slope of the line in Fig. 5, we obtain $r_{Hall} = 0.9$. From Eq. (3) and $r_{Hall} = \mu_{Hall}/\mu$ and the measured slope of the line in Fig. 6 *and* the assumption that $\mu = \mu_{IR}$, we obtain $r_{Hall} = 1.2$. We view the approximate agreement between the two estimates of r_{Hall} as quite reasonable, and both estimates are consistent with previous experiments that support a value close to unity for highly doped p-GaAs.[3,21]

In Fig. 6 we have included our earlier results for μ_{IR} based on the (usual) effective-plasmon model,[3] using Eq. (3) with the effective-plasmon γ_p in place of $\gamma_{plasmon}$. As discussed earlier, the effective-plasmon γ_p is forced to be large (and the corresponding μ_{IR} is forced to be small) in order to encompass both the true-plasmon and the IVB absorption bands; it is this which leads to the discrepancy between the effective-plasmon μ_{IR} and the dc mobility μ_{Hall}. But our results for the true-plasmon μ_{IR}, obtained by separating the plasmon contribution from the intervalenceband one, show that (for highly doped p-GaAs) the actual optical mobility μ_{IR} is close to μ_{Hall}, and that both (because the Hall factor is close to 1.0) provide close approximations to the drift mobility μ.

VII. CONCLUSIONS

We conclude as follows. Using direct numerical-solution techniques for the reflectance and transmittance of a multilayer structure, we have experimentally determined the infrared optical properties of a series of highly doped GaAs:C MBE films. The results reveal (Figs. 2–4) two broad absorption bands in the region in which earlier work using the effective-plasmon model showed only one very broad band. The experimental spectra were analyzed by a combination of intervalenceband and plasmon processes, in which the IVB calculations were carried out using reported GaAs valenceband parameters and Kane's $\mathbf{k}\cdot\mathbf{p}$ method. The $\omega_{plasmon}$ and $\gamma_{plasmon}$ values obtained for the separated-out plasmon contribution, when compared to our Hall results for the hole mobility and carrier concentration (Figs. 5 and 6), show that the Hall factor for highly doped p-GaAs is close to 1.0, consistent with earlier findings. The infrared mobility μ_{IR} corresponding to the actual-plasmon $\gamma_{plasmon}$ (unlike the IVB-entangled effective-plasmon μ_{IR}), is found to be close to the dc mobility μ_{Hall}; there is no significant μ_{IR}/μ_{Hall} discrepancy. As by-products of this work, the (R,T) numerical solutions are found to accurately determine the film thickness, and support is provided for the set of valenceband parameters reported in Ref. 17.

[1] R. Braunstein and E. O. Kane, J. Phys. Chem. Solids **23**, 1423 (1962).

[2] R. Fukasawa, K. Sakai, and S. Perkowitz, Jpn. J. Appl. Phys., Part 1 **36**, 5543 (1997).

[3] W. Songprakob, R. Zallen, W. K. Liu, and K. L. Bacher, Phys. Rev. B **62**, 4501 (2000).

[4] M. L. Huberman, A. Ksendov, A. Larsson, R. Terhune, and J. Maserjian, Phys. Rev. B **44**, 1128 (1991).

[5] D. V. Tsu, J. Vac. Sci. Technol. A **17**, 1854 (1999).

[6] *OptiCon* software, developed at Energy Conversion Devices by D. V. Tsu, uses Digital Visual Fortran under Windows 95.

[7] C. L. Nagendra and G. K. M. Thutupalli, Vacuum **31**, 141 (1981).

[8] D. V. Tsu, J. Vac. Sci. Technol. B **18**, 1796 (2000).

[9] B. Carnanon and J. O. Wilkes, *Digital Computing and Numerical Methods* (Wiley, New York, 1973), p. 368.

[10] J. S. Blakemore, J. Appl. Phys. **53**, R123 (1982).

[11] O. K. Kim and W. G. Spitzer, J. Appl. Phys. **50**, 4362 (1979).

[12] R. Newman and W. W. Tyler, Phys. Rev. **105**, 885 (1957).

[13] E. O. Kane, J. Phys. Chem. Solids **1**, 82 (1956).

[14] P. Pfeffer and W. Zawadzki, Phys. Rev. B **53**, 12813 (1996). Table II of this paper lists GaAs band-structure parameters in terms of the Luttinger parameters ($\gamma_1, \gamma_2, \gamma_3$). The connections between the Luttinger parameters and the Kane parameters (L, M, N) are $L = -(\gamma_1 + 4\gamma_2 + 1)\hbar^2/2m$, $M = -(\gamma_1 - 2\gamma_2 + 1)\hbar^2/2m$, and $N = -6\gamma_3 \hbar^2/2m$ [from O. Madelung, in *Landolt-Börnstein Numerical Data and Functional Relationships in Science and Technology*, edited by O. Madelung (Springer, Berlin, 1982), Vol. 17a, p. 19].

[15] I. Balslev, Phys. Rev. **177**, 1173 (1969).

[16] M. S. Skolnick, A. K. Jain, R. A. Stradling, J. Leotin, J. C. Ousset, and S. Askenazy, J. Phys. C **9**, 2809 (1976).

[17] W. Ekardt, K. Losch, and D. Bimberg, Phys. Rev. B **20**, 3303 (1979).

[18] The theoretical $\alpha(h\nu)$ for each GaAs:C film was derived from $\alpha = 2\omega \, \mathrm{Im}(\epsilon_{film}^{1/2})/c$, where $\epsilon_{film} = \epsilon_{lattice} + 4\pi(\chi_{plasmon} + \chi_{IVB})$. The Drude form $-\epsilon_\infty \omega_{plasmon}^2/(\omega^2 - i\omega\gamma_{plasmon})$ was used for the hole-plasmon susceptibility $4\pi\chi_{plasmon}$. Intervalenceband transitions among the heavy-hole (1), light-hole (2), and split-off (3) bands contribute to the IVB susceptibility: $4\pi\chi_{IVB} = 4\pi(\chi_{21} + \chi_{31} + \chi_{32})$. The χ_{ij} were formulated using an oscillator model in the room-temperature relaxation-time approximation (Ref. 4):

$$\chi_{ij}(\omega) = \frac{4\pi e^2}{m} \sum_{\mathbf{k}} \left(\frac{2m|\mathbf{k}|^2}{\hbar^3 \omega_{ji}} \right) \frac{W_{ij}(\mathbf{k}) f_{ij}}{\omega_{ji}^2 - \omega^2 + i\omega\gamma_{IVB}}.$$

Here $\mathbf{k}$ is the electron wave vector, $W_{ij}(\mathbf{k})$ is the optical matrix element for a direct transition between valence bands i and j, $\hbar\omega_{ji}=E_j(\mathbf{k})-E_i(\mathbf{k})$ is the transition energy, and $f_{ij}=f(E_i)-f(E_j)$ is the difference between the room-temperature Fermi–Dirac occupation probabilities. The matrix elements $W_{ij}(\mathbf{k})$ were calculated from analytic expressions given by Kane (Ref. 13) for $\mathbf{k}\|[100]$, $\mathbf{k}\|[110]$, and $\mathbf{k}\|[111]$. We then averaged over these three directions with weights of 0.27, 0.46, and 0.27, respectively. (We used a similar approach for the three valence band energies E_i, after solving the eigenenergy secular equations given in Ref. 13.) Our averaging approach, applied in this isotropic-band approximation, differs somewhat from that in Ref. 13.

[19] J. D. Wiley, and M. DiDomenico, Phys. Rev. B **2**, 427 (1970); J. D. Wiley, in *Semiconductors and Semimetals*, edited by R. K. Willardson and A. C. Beer (Academic, New York, 1975), Vol. 10, p. 91.

[20] E. Conwell, in *Handbook on Semiconductors*, edited by W. Paul (North-Holland, New York, 1982), Vol. 1, pp. 530–539; B. W. Kim and A. Majerfeld, J. Appl. Phys. **79**, 1939 (1996).

[21] M. Wenzel, G. Irmer, J. Monecke, and W. Siegel, J. Appl. Phys. **81**, 7810 (1997); Semicond. Sci. Technol. **13**, 505 (1998). Figure 6 in the former paper and Fig. 4(a) in the latter show that the Hall mobility and the drift mobility coincide at high doping, where ionized impurity scattering is dominant.